Site Valencies and Spin Coupling in the 3Fe and 4Fe ($S = 1/2$) Clusters of *Pyrococcus furiosus* Ferredoxin by ^{57}Fe ENDOR

Joshua Telser,[§,‡] Heshu Huang,[†] Hong-In Lee,[§] Michael W. W. Adams,*[,†] and Brian M. Hoffman*[,§]

Contribution from the Department of Chemistry, Northwestern University, Evanston, Illinois 60208-3113, and the Department of Biochemistry & Molecular Biology and the Center for Metalloenzyme Studies, University of Georgia, Athens, Georgia 30602-2556

Received May 12, 1997. Revised Manuscript Received November 25, 1997

Abstract: The hyperthermophilic archaeon *Pyrococcus furiosus* contains a novel ferredoxin (*Pf*-Fd) in which, in the native 4Fe form, three of the Fe ions are coordinated to the protein by cysteinyl thiolato ligands, but the fourth, labile, Fe is coordinated by an aspartyl carboxalato ligand. Addition of excess cyanide ion to the reduced 4Fe protein, *Pf*-Fd 4Fe-red, yields a species with EPR properties that differ greatly from the native cluster form (*Pf*-Fd 4Fe−CN). The unique Fe can be removed, to form a 3Fe cluster, which in turn can be reconstituted to regenerate the 4Fe form. The lability of this fourth Fe allows the preparation of a series of ^{57}Fe cluster isotopologs: *Pf*-Fd 3Fe-ox ($S = 1/2$) as $[Fe_3S_4]^+$ and $[^{57}Fe_3S_4]^+$; *Pf*-Fd 4Fe-red as $[Fe_4S_4]^+$, $[^{57}FeFe_3S_4]^+$, and $[Fe^{57}Fe_3S_4]^+$ as well as the corresponding ^{57}Fe isotopologs of *Pf*-Fd 4Fe−CN. The 3Fe and 4Fe cluster-containing native and cyanide-bound forms all have been investigated by ^{57}Fe ENDOR spectroscopy at cryogenic temperatures. The ground state of *Pf*-Fd 3Fe-ox is similar to that seen for other 3Fe Fd's but shows evidence of less symmetrical intracluster spin-coupling. The theoretical framework created by earlier studies, particularly those of Noodleman and co-workers (Mouesca, J.-M.; Noodleman, L.; Case, D. A.; Lamotte, B. *Inorg. Chem.* **1995**, *34*, 4347−4359), allows us to use ^{57}Fe ENDOR data alone to characterize the spin-coupling within both the native and cyanide-bound $S = 1/2$ forms of *Pf*-Fd 4Fe-red. This procedure shows that cyanide binding to the unique Fe ion causes it to undergo a "valency switch" from $Fe^{2.5+}$ to Fe^{2+}. The interchange also is detected by NMR analysis (Calzolai et al. *J. Am. Chem. Soc.* **1997**, *119*, 9341−9350). We find that the cyanide-bound cluster has a spin state common to many $[Fe_4S_4]^+$ clusters, whereas the native form may exhibit a previously unidentified spin-coupling ground state.

Introduction

Iron−sulfur proteins[1] are found in a wide variety of organisms and play diverse functional roles including electron transfer and chemical catalysis.[2−12] Other roles, including structural,[13] regulatory,[14,15] iron storage,[16] generation/stabilization of radical intermediates,[17,18] and site specific sulfide chemistry[19] have also been proposed.

Ferredoxins (Fd's)[1] containing three or four Fe ions in "precubane" $[Fe_3S_4]^{n+}$ or cubane-type $[Fe_4S_4]^{n+}$ clusters, respectively, comprise one of the most important classes of Fe−S proteins.[2,3] The cluster is normally bound to protein via four cysteinyl residues in 4Fe Fd's; in 3Fe−Fd's, the fourth cysteine is generally available for binding to Fe upon conversion to a 4Fe cluster. Although the precubane $[Fe_3S_4]$ cluster can be generated from a 4Fe cluster in some cases as a nonphysiological variant, it is also found to be the functionally relevant cluster form in such enzymes as succinate dehydrogenase and fumarate reductase.[2,3] Proteins with the cubane 4Fe cluster can also have catalytic roles, primarily as hydrolase enzymes.[11,20−25] These

[†] University of Georgia.

[§] Northwestern University.

[‡] Permanent address: Chemistry Program, Roosevelt University, 430 S. Michigan Ave., Chicago, IL 60605-1394.

(1) Abbreviations used: CW, continuous wave; EPR, electron paramagnetic resonance; ENDOR, electron nuclear double resonance; ESE, electron spin−echo; ESEEM, electron spin−echo envelope modulation; Fd, ferredoxin; hwhm, half-width at half-maximum; MCD, magnetic circular dichroism; *Pf*, *Pyrococcus furiosus*; *Pf*-Fd 3Fe-ox: form of the protein containing the $[Fe_3S_4]^+$ cluster; *Pf*-Fd 3Fe-red: form of the protein containing the $[Fe_3S_4]^0$ cluster; *Pf*-Fd 4Fe-red: form of the protein containing the $[Fe_4S_4]^+$ cluster; *Pf*-Fd 4Fe−CN: form of the protein containing the $[Fe_4S_4]^+$ cluster with CN^- bound to the labile Fe ion; Rd, rubredoxin; rf, radio frequency; RR, resonance Raman.

(2) Johnson, M. K. In *Encyclopedia of Inorganic Chemistry*; King, R. B., Ed.; Wiley: UK, 1994; Vol. 4, pp 1896−1915.
(3) Cammack, R. *Adv. Inorg. Chem.* **1992**, *38*, 281−322.
(4) *Iron Sulfur Proteins*; Lovenberg, W., Ed.; Academic Press: New York, 1973−1977; Vol. I−III.
(5) *Iron Sulfur Proteins*; Spiro, T. G., Ed.; Wiley: New York, 1982.
(6) *Metal Clusters in Proteins*; Que, L., Jr., Ed.; ACS Symposium Series 372; American Chemical Society: Washington, DC, 1988.
(7) Lindahl, P. A.; Kovacs, J. A. *J. Cluster Sci.* **1990**, *1*, 29−73.
(8) Ohnishi, T. *Curr. Top. Bioenerg.* **1987**, *15*, 37−65.
(9) Golbeck, J. H. *Biochim. Biophys. Acta* **1987**, *895*, 167−204.
(10) Beinert, H. *FASEB J.* **1990**, *4*, 2483−2491.
(11) Beinert, H.; Kennedy, M. C. *Eur. J. Biochem.* **1989**, *186*, 5−15.
(12) Kennedy, M. C.; Stout, C. D. *Adv. Inorg. Chem.* **1992**, *38*, 323−339.
(13) Kuo, C.-F.; McRee, D. E.; Fisher, C. L.; O'Handley, S. F.; Cunningham, R. P.; Rainer, J. A. *Science* **1992**, *258*, 434−440.
(14) Rouault, T. A.; Stout, D. C.; Kaptain, S.; Harford, J. B.; Klausner, R. D. *Cell* **1991**, *64*, 881−883.
(15) Switzer, R. L. *BioFactors* **1989**, *2*, 77−86.
(16) Thauer, R. K.; Schönheit, P. In *Iron Sulfur Proteins*; Spiro, T. G., Ed.; Wiley: New York, 1982; pp 329−341.
(17) Frey, P. A.; Reed, G. H. *Adv. Enzymol.* **1993**, *66*, 1−39.
(18) Reichard, P. *J. Biol. Chem.* **1993**, *31*, 8383−8386.
(19) Staples, C. R.; Ameyibor, E.; Fu, W.; Gardetsalvi, L.; Strittetter, A. L.; Schurmann, P.; Knaff, D. B.; Johnson, M. K. *Biochemistry* **1996**, *35*, 11425−11434.
(20) Flint, D. H.; Emptage, M. H.; Finnegan, M. G.; Fu, W.; Johnson, M. K. *J. Biol. Chem.* **1993**, *268*, 14732−14742.

S0002-7863(97)01546-1 CCC: $15.00
Published on Web 01/27/1998

enzymes do not contain a symmetrically ligated $[Fe_4S_4]$ cluster but rather a catalytically active, asymmetrically ligated cluster created by removal of a cysteinyl ligand and its replacement by a more labile (exogenous or endogenous) ligand. The prototypical example is aconitase, in which one of the Fe atoms of its single $[Fe_4S_4]$ cluster is coordinated by hydroxide in its resting state, but binds and activates substrate during enzymatic action.[11,12,26,27]

The asymmetric cluster found in catalytic Fe−S enzymes can be generated in small molecules[28−30] and is also found in certain electron-transfer Fe−S proteins. The ferredoxin isolated from the hyperthermophilic archaeon *Pyrococcus furiosus* (*Pf*-Fd) is one such protein.[31−35] It is a small and monomeric Fd (M_r 7500), containing a single $[Fe_4S_4]$ cluster bound by only three cysteinyl residues (Cys-11, Cys-17, Cys-56).[31−33] The fourth cluster ligand is a carboxylate of asparate (Asp-14).[36] The carboxylate-bound Fe can be removed to form a 3Fe cluster whose $[Fe_3S_4]$ $S = 2$ reduced form has been studied by Mössbauer spectroscopy.[37] Addition of excess cyanide ion to the 4Fe form leads to binding of a single CN^- to the unique Fe and a putative loss of the carboxylate ligand, with dramatic changes in the cluster's MCD and EPR spectrum.[38] A recent electron nuclear double resonance (ENDOR) spectroscopic study of the reduced form of *Pf*-Fd (*Pf*-Fd 4Fe-red, $[Fe_4S_4]^+$, $S = 1/2$ state) in the presence and absence of cyanide ion showed that the reduced cyanide-bound form (*Pf*-Fd 4Fe−CN) electronically and geometrically resembled a $[Fe_4S_4]^+$ with complete cysteinyl ligation.[39] ^{13}C and ^{15}N ENDOR spectroscopy of cluster-bound CN^- isotopologs showed isotropic hyperfine couplings much smaller than those for cyanide bound to monomeric metal sites.[39]

To extend that earlier study with a characterization of the spin coupling within this cluster, we use ^{57}Fe ENDOR of ^{57}Fe-enriched isotopologs of both the 4Fe-red and 3Fe-ox ($[Fe_3S_4]^+$, $S = 1/2$) forms. These enriched samples are prepared by an approach first employed with the analogous protein, aconitase.[40] The 4Fe−Fd is converted to the 3Fe form and ^{57}Fe is added under reducing conditions to yield the "locally" enriched $[^{57}Fe_aFe_3S_4]^+$ cluster. Although it is comparatively easy to grow *P. furiosus* on ^{57}Fe-enriched medium, compared to the bovine source of aconitase, we have followed the pioneering work of Beinert and Kennedy[11] and prepared apo-*Pf*-Fd. Reconstitution of holoenzyme with ^{57}Fe yields the "globally" enriched $[^{57}Fe_4S_4]^+$ cluster. Conversion to 3Fe−Fd yields the $[^{57}Fe_3S_4]^+$ cluster (which can be reduced to the $[^{57}Fe_3S_4]^0$ cluster), and addition of natural isotopic abundance Fe under reducing conditions yields the $[Fe_a{}^{57}Fe_3S_4]^+$ cluster. Thus, a complete series of ^{57}Fe isotopologs can be generated for study by ENDOR spectroscopy.

Extensive Mössbauer[37,41−47] and also ENDOR studies[40,48−55] of the ^{57}Fe sites of the Fe−S proteins and model compounds,[56] paralleled by numerous, detailed theoretical studies have given a firm foundation for our understanding of the electronic structure of Fe−S clusters.[44,57−65] The $S = 1/2$ electronic ground state of oxidized 3Fe Fd's arises from magnetic coupling among the three high-spin ($S = 5/2$) Fe^{3+} ions as originally described by Kent et al.[57] In this report we determine ^{57}Fe hyperfine

(21) Scopes, R. K.; Griffiths-Smith, K. *Analytical Biochem.* **1984**, *136*, 530−534.
(22) Dreyer, J.-L. *Eur. J. Biochem.* **1985**, *150*, 145−150.
(23) Kuchta, R. D.; Hanson, G. R.; Holmquist, B.; Abeles, R. H. *Biochemistry* **1986**, *25*, 7301−7307.
(24) Flint, D. H.; Emptage, M. H.; Guest, J. R. *Biochemistry* **1992**, *31*, 10331−10337.
(25) Flint, D. H.; Emptage, M. H. *J. Biol. Chem.* **1988**, *263*, 3558−3564.
(26) Werst, M. M.; Kennedy, M. C.; Beinert, H.; Hoffman, B. M. *Biochemistry* **1990**, *29*, 10526−10532.
(27) Robbins, A. H.; Stout, C. D. *Proteins: Struct., Funct., Genet.* **1989**, *5*, 289−312.
(28) Holm, R. H.; Ciurli, S.; Weigel, J. A. *Prog. Inorg. Chem.* **1990**, *38*, 1−74.
(29) Holm, R. H. *Adv. Inorg. Chem.* **1992**, *38*, 1−71.
(30) Carney, M. J.; Papaefthymiou, G. C.; Spartalian, K.; Frankel, R. B.; Holm, R. H. *J. Am. Chem. Soc.* **1988**, *110*, 6084−6095.
(31) Aono, S.; Bryant, F. O.; Adams, M. W. W. *J. Bacteriology* **1989**, *171*, 3433−3439.
(32) Conover, R. C.; Kowal, A. T.; Fu, W.; Park, Jae-B.; Aono, S.; Adams, M. W. W.; Johnson, M. K. *J. Biol. Chem.* **1990**, *265*, 8533−8541.
(33) Busse, S. C.; La Mar, G. N.; Yu, L. P.; Howard, J. B.; Smith, E. T.; Zhou, Z. H.; Adams, M. W. W. *Biochemistry* **1992**, *31*, 11952−11962.
(34) Adams, M. W. W. *Annu. Rev. Microbiol.* **1993**, *47*, 627−658.
(35) Adams, M. W. W. *Adv. Inorg. Chem.* **1992**, *38*, 341−396.
(36) Calzolai, L.; Gorst, C. M.; Zhao, Z.-H.; Teng, Q.; Adams, M. W. W.; La Mar, G. N. *Biochemistry* **1995**, *34*, 11373−11384.
(37) Srivastava, K. K. P.; Surerus, K. K.; Conover, R. C.; Johnson, M. K.; Park, J.-B.; Adams, M. W. W.; Münck, E. *Inorg. Chem.* **1993**, *32*, 927−936.
(38) Conover, R. C.; Park, J.-B.; Adams, M. W. W.; Johnson, M. K. *J. Am. Chem. Soc.* **1991**, *113*, 2799−2800.
(39) Telser, J.; Smith, E. T.; Adams, M. W. W.; Conover, R. C.; Johnson, M. K.; Hoffman, B. M. *J. Am. Chem. Soc.* **1995**, *117*, 5133−5140.
(40) Werst, M. M.; Kennedy, M. C.; Houseman, A. L. P.; Beinert, H.; Hoffman, B. M. *Biochemistry* **1990**, *29*, 10533−10540.
(41) Trautwein, A. X.; Bill, E.; Bominaar, E. L.; Winkler, H. *Struct. Bonding* **1991**, *78*, 1−95.
(42) Hu, Z.; Jollie, D.; Burgess, B. K.; Stephens, P. J.; Münck, E. *Biochemistry* **1994**, *33*, 14475−14485.
(43) Huynh, B. H.; Patil, D. S.; Moura, I.; Teixeira, M.; Moura, J. J. G.; DerVartanian, D. V.; Czechowski, M. H.; Prickril, B. C.; Peck, H. D., Jr.; LeGall, J. *J. Biol. Chem.* **1987**, *262*, 795−800.
(44) Papaefthymiou, V.; Girerd, J.-J.; Moura, I.; Moura, J. J. G.; Münck, E. *J. Am. Chem. Soc.* **1987**, *109*, 4703−4710.
(45) Auric, P.; Gaillard, J.; Meyer, J.; Moulis, J.-M. *Biochem. J.* **1987**, *242*, 525−530.
(46) Lindahl, P. A.; Day, E. P.; Kent, T. A.; Orme-Johnson, W. H.; Münck, E. *J. Biol. Chem.* **1985**, *260*, 11160−11173.
(47) Middleton, P.; Dickson, D. P.; Johnson, C. E.; Rush, J. D. *Eur. J. Biochem.* **1978**, *88*, 135−141.
(48) Moura, I.; Macedo, A.; Moura, J. J. G. In *Advanced EPR: Applications in Biology and Biochemistry*; Hoff, A. J., Ed.; Elsevier: Amsterdam, 1989; pp 813−838.
(49) Hoffman, B. M.; DeRose, V. J.; Doan, P. E.; Gurbiel, R. J.; Houseman, A. L. P.; Telser, J. In *EMR of Paramagnetic Molecules*; Biological Magnetic Resonance 13; Berliner, L. J., Reuben, J., Eds.; Plenum Press: New York, 1993; Chapter 4, pp 151−218.
(50) Hoffman, B. M. *Acc. Chem. Res.* **1991**, *24*, 164−170.
(51) Hoffman, B. M.; Gurbiel, R. J.; Werst, M. M.; Sivaraja, M. In *Advanced EPR. Applications in Biology and Biochemistry*; Hoff, A. J., Ed.; Elsevier: Amsterdam, 1989; Chapter 15, pp 541−591.
(52) Lowe, D. J. *Prog. Biophys. Mol. Biol.* **1992**, *57*, 1−22.
(53) Sands, R. H. In *Multiple Electron Resonance Spectroscopy*; Dorio, M. M., Freed, J. H., Eds.; Plenum Press: New York and London, 1979; Chapter 9, pp 331−374.
(54) Anderson, R. E.; Anger, G.; Petersson, L.; Ehrenberg, A.; Cammack, R.; Hall, D. O.; Mullinger, R.; Rao, K. K. *Biochim. Biophys. Acta* **1975**, *376*, 63−71.
(55) Orme-Johnson, W. H.; Sands, R. H. In *Iron−Sulfur Proteins*; Lovenberg, W., Ed.; Academic Press: New York, 1973; Vol. II, pp 195−238.
(56) Rius, G.; Lamotte, B. *J. Am. Chem. Soc.* **1989**, *111*, 2464−2469.
(57) Kent, T. A.; Huynh, B. H.; Münck, E. *Proc. Natl. Acad. Sci. U.S.A.* **1980**, *77*, 6574−6576.
(58) Borshch, S. A.; Bominaar, E. L.; Blondin, G.; Girerd, J.-J. *J. Am. Chem. Soc.* **1993**, *115*, 5155−5168.
(59) Guigliarelli, B.; More, C.; Bertrand, P.; Gayda, J. P. *J. Chem. Phys.* **1986**, *85*, 2774−2778.
(60) Mouesca, J.-M.; Noodleman, L.; Case, D. A.; Lamotte, B. *Inorg. Chem.* **1995**, *34*, 4347−4359.
(61) Mouesca, J.-M.; Chen, J. L.; Noodleman, L.; Bashford, D.; Case, D. A. *J. Am. Chem. Soc.* **1994**, *116*, 11898−11914.
(62) Noodleman, L. *Inorg. Chem.* **1991**, *30*, 246−256.
(63) Noodleman, L. *Inorg. Chem.* **1991**, *30*, 256−264.
(64) Noodleman, L.; Peng, C. Y.; Case, D. A.; Mouesca, J.-M. *Coord. Chem. Rev.* **1995**, *144*, 199−244.
(65) Noodleman, L.; Case, D. A. In *Iron−Sulfur Proteins*; Advances in Inorganic Chemistry Vol. 38; Cammack, R., Ed.; Academic Press: San Diego, 1992; pp 423−470.

coupling tensors for *Pf*-Fd 3Fe-ox and use them within this model to discuss the exchange interactions among the ferric ions.

In reduced 4Fe Fd ($[Fe_4S_4]^+$) clusters there are formally three ferrous and one ferric ion, but it has been shown that double-exchange between a "ferrous" and a "ferric" ion leads to formation of a valence-delocalized, or mixed-oxidation state, $(Fe^{2.5+})_2$ pair, while the other two iron ions form a "ferrous pair".[44,58,66,67] Magnetic coupling among these paired ions typically leads to an $S = 1/2$ electronic ground state, with higher spin states also observed. The theoretical framework created by these studies, particularly those of Noodleman and co-workers,[60−65] allows us to use ^{57}Fe ENDOR data to characterize the spin-coupling scheme within both the native and cyanide-bound $S = 1/2$ forms of *Pf*-Fd 4Fe-red. This procedure shows that cyanide binding to the unique Fe ion causes it to undergo a "valency switch" from $Fe^{2.5+}$ to Fe^{2+}. We find that the cyanide-bound cluster has a spin state common to many $[Fe_4S_4]^+$ clusters, while the native form may exhibit a previously unidentified spin-coupling ground state.

Experimental Section

Holoprotein Preparation. *Pf*-Fd was isolated under anaerobic conditions in the presence of 2 mM sodium dithionite as described previously.[31] Samples for spectroscopic studies were in 50 mM Tris/HCl buffer, pH 7.8 with 2 mM dithionite. Sample concentrations were based on the molar absorption coefficient at 390 nm, $\epsilon_{390} = 17\,000$ M^{-1} cm^{-1}, for air-oxidized samples.[32] Samples for ENDOR were typically 1 mM in Fd, and cyanide-treated samples were incubated for 2 h with a 250-fold molar excess of a neutral solution of KCN.[38]

Preparation of Isotopologs. All procedures were carried out under anaerobic conditions unless otherwise specified, and the buffer used throughout was 50 mM Tris/HCl. Apo*Pf*-Fd was prepared as follows: the protein (3 mg/mL) was precipitated twice with trichloroacetic acid (10%) with resuspension in buffer, pH 8.0, and was finally dissolved in buffer containing 100 mM 2-mercaptoethanol. The protein was desalted using a Sephadex G-25 column (2.6 × 32 cm) equilibrated with buffer. To reconstitute the 4Fe-form, apo*Pf*-Fd was incubated with a 20-fold molar excess of dithiothreitol in buffer (pH 7.4) for 16 h, the same molar excess of Na_2S and Fe^{2+} (see below) was added, and the solution was incubated for a further 1 h. The mixture was applied to the Sephadex G-25 column equilibrated with buffer containing 2 mM sodium dithionite and 200 mM NaCl at pH 8.0, and the Fd-containing fractions were concentrated using ultrafiltration (Amicon YM3). Natural abundance Fe^{2+} was supplied as ferrous chloride, and $^{57}Fe^{2+}$ was prepared by dissolving the metal in 1:3 HNO_3/HCl and adjusting to pH 4.0 with NaOH. The 3Fe-form was prepared as previously described.[32] The conversion to the 4Fe-form was carried out by incubation of the protein (3 mg/mL) in buffer with a 20-fold molar excess of Fe^{2+} for 3 h followed by gel filtration and ultrafiltration as described above. Samples for spectroscopic analyses were prepared in buffer (pH 8.0) containing 30% (v/v) ethylene glycol.

EPR and ENDOR Studies. CW "Q"-band (35 GHz) EPR/ENDOR spectra were recorded on a modified Varian E−109 spectrometer at 2 K in the dispersion mode using 100 kHz field modulation. Under these "rapid-passage" conditions, the EPR spectra represent the actual absorption envelope,[68−71] as seen in Figure 1, not its derivative as is typically the case. CW ^{57}Fe ENDOR signals were enhanced by application of rf broadening as described previously.[72]

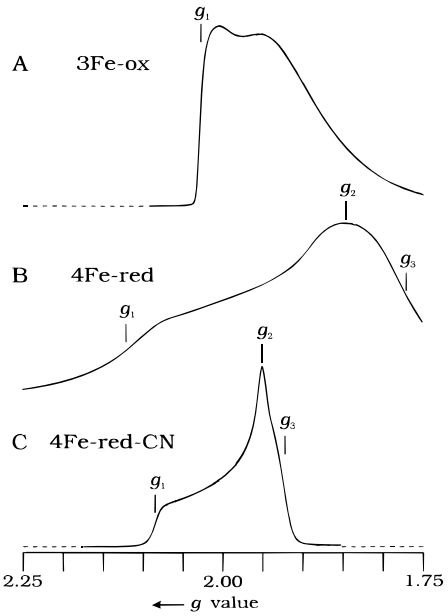

Figure 1. Q-band CW EPR spectra of *Pf*-Fd: (A) *Pf*-Fd 3Fe-ox, (B) *Pf*-Fd 4Fe-red, (C) *Pf*-Fd 4Fe−CN. *Experimental conditions*: (A) temperature, 2 K; microwave frequency, 34.987 GHz; microwave power, 20 μW (40 dBm); 100 kHz field modulation amplitude, 0.13 mT; time constant, 32 ms; (B) as in (A) except: microwave frequency, 35.040 GHz; (C) as in (A) except: microwave frequency, 34.905 GHz; microwave power, 2 μW (50 dBm). The canonical g values are indicated for each spectrum, where determinable.

We find that a combination of electron-spin and nuclear-spin relaxation effects makes the phase and line shape of the ^{57}Fe CW ENDOR signals in *Pf*-Fd extremely sensitive to experimental conditions, chiefly field modulation amplitude and rf sweep directions. We have previously observed these effects in other Fe−S proteins.[49−51,73] As seen in the Supporting Information (see Figures S1 and S4), these phenomena actually can aid in identifying and classifying the individual resonant frequencies of CW ^{57}Fe ENDOR spectra that are superpositions of signals from multiple sites.

Pulsed Q-band and X-band (∼9.5 GHz) spectra were recorded on locally built spectrometers that have been previously described.[51,74,75] Pulsed ^{57}Fe ENDOR spectra were recorded at either 2 or 4.2 K using the Davies[76] pulse sequence, appropriate for larger hyperfine couplings (A > 8 MHz). In this sequence, the ENDOR response depends on the product of A and the preparation pulse width t_p, with the maximum intensity at A (MHz)·t_p (μs) ≈ 0.7.[74,76−78] Thus $t_p \approx 0.05$ μs was chosen so as to enhance the ^{57}Fe X-band Davies ENDOR signals ($A(^{57}Fe)$ = 20−30 MHz; $A \cdot t_p \approx 1$) while suppressing the overlapping ^{1}H pattern ($A(^1H) \leq 5$ MHz; $A \cdot t_p < 0.2$). Contrary to the conventional expectation that pulsed ENDOR results do not exhibit the complications of the CW methods, the pulsed (Davies and Mims) spectra of *Pf*-Fd also exhibit opposite phase behavior for different Fe sites within a given spectrum. Similar effects have been observed in ^{57}Fe pulsed 95 GHz ENDOR of Fe sites in zeolites,[79] demonstrating that these phenomena are not unique to aqueous protein ENDOR solutions.

(66) Girerd, J. J. *J. Chem. Phys.* **1983**, *79*, 1766−1775.
(67) Bominaar, E. L.; Borshch, S. A.; Girerd, J. J. *J. Am. Chem. Soc.* **1994**, *16*, 5362−5372.
(68) Mailer, C.; Taylor, C. P. S. *Biochim. Biophys. Acta* **1973**, *322*, 195−203.
(69) Hyde, J. S. *Phys. Rev.* **1960**, *119*, 1483−1492.
(70) Hyde, J. S. *Phys. Rev.* **1960**, *119*, 1492−1495.
(71) Portis, A. M. *Phys. Rev.* **1956**, *104*, 584−588.
(72) Hoffman, B. M.; DeRose, V. J.; Ong, J. L.; Davoust, C. E. *J. Magn. Reson., Ser. A* **1994**, *110*, 52−57.
(73) Hoffman, B. M.; Martinsen, J.; Venters, R. A. *J. Magn. Reson.* **1984**, *59*, 110−123.
(74) Fan, C.; Doan, P. E.; Davoust, C. E.; Hoffman, B. M. *J. Magn. Reson.* **1992**, *98*, 62−72.
(75) Davoust, C. E.; Doan, P., E.; Hoffman, B. M. *J. Magn. Reson., A* **1996**, *119*, 38−44.
(76) Davies, E. R. *Phys. Lett.* **1974**, *47A*, 1−2.
(77) Doan, P. E.; Fan, C.; Davoust, C. E.; Hoffman, B. M. *J. Magn. Reson.* **1991**, *95*, 196−200.
(78) Doan, P. E.; Fan, C.; Hoffman, B. M. *J. Am. Chem. Soc.* **1994**, *116*, 1033−1041.
(79) Goldfarb, D.; Strohmaier, K. G.; Vaughan, D. E. W.; Thomann, H.; Poluetkov, O. G.; Schmidt, J. *J. Am. Chem. Soc.* **1996**, *118*, 4665−4671.

The single-crystal ENDOR transition frequencies for a nucleus, *J*, of spin $I = 1/2$, with low g_N such as ^{57}Fe are given to first order by eq 1[80]

$$\nu_{\pm} = |A^J/2 \pm \nu_J| \quad (1)$$

where A^J is the orientation-dependent nuclear hyperfine coupling constant and ν_J is the nuclear Larmor frequency. For $\nu_J < A^J/2$, as is generally the case for ^{57}Fe, the ENDOR spectrum consists of a Larmor-split doublet centered at $A^J/2$. Computer simulation and analysis of frozen-solution ENDOR spectra employed procedures and programs described elsewhere.[49−51,73,81] Computer simulation of EPR spectra employed the program QPOWA.[82]

Results and Discussion

EPR of $S = 1/2$ *Pf*-Fd Species. Figure 1 presents EPR spectra of the following protein forms: *Pf*-Fd 3Fe-ox, *Pf*-Fd 4Fe-red, and *Pf*-Fd 4Fe−CN. As described in the Experimental Section, such spectra represent the EPR absorption envelope, rather than its derivative. EPR spectra of these paramagnetic forms of *Pf*-Fd have been previously reported;[38,39] however, to aid in discussion of the ENDOR results, we describe them here as well.

The $S = 1/2$ electronic ground state of oxidized 3Fe Fd's arises from magnetic coupling among the three high-spin Fe^{3+} ions. Despite the formal equivalence of these ions, there is often found a distribution in single Fe^{3+} ion zero-field splitting (D) and exchange coupling parameters (J).[59,83,84] This parameter distribution, which results from different conformational substates of the protein,[85] can lead to 3Fe Fd's that lack a well-defined $\boldsymbol{g}$ tensor but instead exhibit a distribution in tensor values. This distribution appears to be particularly broad for *Pf*-Fd 3Fe-ox. As seen in Figure 1A, the "tail" of the EPR signal extends to $g < 1.75$, the magnet cutoff, as opposed to ∼1.9 for *D. gigas* hydrogenase 3Fe form 2 (*Dg*-H_2ase-2) that itself exhibits a significant $\boldsymbol{g}$ distribution,[84] although the single well-defined g value, g_1, is quite similar for the two proteins ($g_1 = 2.030$ for *Pf*-Fd versus 2.032 and 2.029 for *Dg*-H_2ase forms 1 and 2, respectively).

In a frozen solution of *Pf*-Fd 4Fe-red, the majority of the reduced 4Fe Fd ($[Fe_4S_4]^+$) cluster is in an $S = 3/2$ state, with <20% in the $S = 1/2$ state whose spectrum is shown. The two are not in equilibrium as temperature variation does not change their relative amounts.[38] The relative amounts are somewhat sensitive to the amount of glassing agent in the solvent. Unfortunately, the glassing agent required for ENDOR spectroscopy leads to a particularly low fraction of protein in the $S = 1/2$ state (∼10%) so that quite concentrated protein solutions exhibit a very low signal intensity of the $S = 1/2$ state. The existence of the $S = 3/2$ state in high concentration does not contribute to the EPR spectra at 2 K with dispersion mode detection under rapid passage conditions, as the $S = 3/2$ form is barely observable when low microwave power is used (∼20 μW) as in the present study. It is likely that the two spin states represent slightly different conformations "locked in" by freezing. Recent NMR studies have shown no evidence for an accessible $S = 3/2$ state in liquid solution; the observed paramagnetic shifts arise solely from an $S = 1/2$ cluster spin state.[36] The ENDOR results described here are exclusively for this lower spin state, which has $\boldsymbol{g} = [2.105(5), 1.855(5), 1.775(5)]$ (Figure 1B; $\boldsymbol{g}$ tensors and EPR line widths of $[Fe_4S_4]^+$ systems are summarized in Table SI). The very broad single-crystal EPR line widths ($\boldsymbol{W} \approx$ [700, 600, 600] MHz, Gaussian, hwhm; determined by EPR simulation;[82] line widths are summarized in Table SI) for this species suggest that significant protein conformational distribution obtains even in the $S = 1/2$ 4Fe form. This conformational distribution may arise from the Asp carboxylato ligand being less effective than a Cys thiolato ligand at "locking in" a given protein conformation about the cluster. This in turn may be a consequence of the ability of a carboxylato ligand to exhibit either η^1- or η^2-coordination (or intermediate coordination mode) to the labile Fe. Indeed, it has been suggested from NMR analyses that the aspartyl coordination mode may be dependent upon cluster oxidation state.[36]

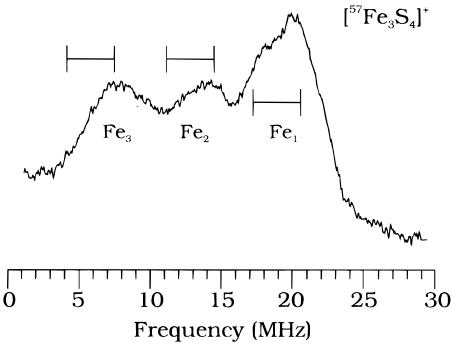

Figure 2. Q-Band CW ^{57}Fe ENDOR of fully labeled *Pf*-Fd 3Fe-ox, $[^{57}Fe_3S_4]^+$. The "goalposts" correspond to $2\nu(^{57}Fe) = 3.38$ MHz and are positioned at the ν_+ branches of the three Fe sites (ν_- is identifiable only for Fe_1). *Experimental conditions*: temperature, 2 K; microwave frequency, 35.028 GHz; microwave power, 6.3 μW (45 dBm); magnetic field, 1.2280 T ($g = 2.038$, g_1); 100 kHz field modulation amplitude, 0.05 mT; time constant, 32 ms; rf scan rate, −1 MHz/s; rf power, 20 W; number of scans, 50.

As described previously,[38,39] addition of excess cyanide ion profoundly changes the electronic properties of *Pf*-Fd 4Fe-red. The cluster is quantitatively converted to a new $S = 1/2$ state, with a well-defined $\boldsymbol{g} = [2.0885(5), 1.952(1), 1.924(1)]$ as shown in Figure 1C. In contrast to *Pf*-Fd 4Fe-red, the single-crystal EPR line widths are quite narrow in the cyanide-bound form ($\boldsymbol{W} =$ [130, 70, 150] MHz, Gaussian, hwhm; determined by EPR simulation[82]). ENDOR analysis of the cyano ligand using $^{13}CN^-$ and $C^{15}N^-$ and comparison with model compounds showed that with a fourth, unidentate, strong-field ligand, *Pf*-Fd 4Fe−CN resembles a conformationally rigid, "normal" $[Fe_4S_4(SR)_4]^{3-}$ cluster.[39]

^{57}Fe ENDOR of *Pf*-Fd 3Fe-ox. Figure 2 presents "single crystal-like" CW 35 GHz ^{57}Fe ENDOR spectrum of the fully labeled *Pf*-Fd-3Fe-ox $[^{57}Fe_3S_4]^+$ cluster as taken under optimized spectrometer conditions (see Experimental Section and Figure S1) at a magnetic field position corresponding to the single well-defined g value, $g_1 = 2.030$. A strong ^{57}Fe signal is seen at 4−24 MHz, that is absent in the natural-abundance sample. No other signals are observed for this globally enriched sample except those assignable to ^{1}H, which are identical with those seen for the natural-abundance sample.[86] As indicated in the

(80) Abragam, A.; Bleaney, B. *Electron Paramagnetic Resonance of Transition Ions*, 2nd ed.; Clarendon Press: Oxford, 1970.
(81) Hoffman, B. M.; Venters, R. A.; Martinsen, J. *J. Magn. Reson.* **1985**, *62*, 537−542.
(82) Belford, R. L.; Belford, G. G. *J. Chem. Phys.* **1973**, *59*, 853−854.
(83) Guigliarelli, B.; Gayda, J. P.; Bertrand, P.; More, C. *Biochim. Biophys. Acta* **1986**, *871*, 149−155.
(84) Fan, C.; Houseman, A. L. P.; Doan, P.; Hoffman, B. M. *J. Phys. Chem.* **1993**, *97*, 3017−3022.
(85) Frauenfelder, H.; Sligar, S. G.; Wolynes, P. G. *Science* **1991**, *254*, 1598−1603.
(86) Fu, W.; Telser, J.; Hoffman, B. M.; Smith, E. T.; Adams, M. W. W.; Finnegan, M. G.; Conover, R. C.; Johnson, M. K. *J. Am. Chem. Soc.* **1994**, *116*, 5722−5729.

figure, the spectrum is the superposition of signals from each of the three Fe sites, with $|A(^{57}Fe_1)| = 37.5(1.0)$ MHz, $|A(^{57}Fe_2)| \approx 26(2)$ MHz, and $|A(^{57}Fe_3)| \approx 11(2)$ MHz. The extreme distribution in $\boldsymbol{g}$ tensor values in *Pf*-Fd 3Fe-ox prevents a determination of the complete $\boldsymbol{A}(^{57}Fe)$ tensors for its Fe sites by analysis of the field dependent (orientation selected) ^{57}Fe ENDOR pattern, as was done for *Dg*-H_2ase-1.[84] Analysis of spin coupling requires A_{iso} derived from the full tensors, and these can be estimated from the available data with adequate precision. The intrinsic hyperfine anisotropy for monomeric high-spin Fe^{3+} is relatively small (~5% for the single Fe^{3+} in a rubredoxin[57]) and in $[Fe_3S_4]^+$ clusters, the Fe_1 site (that with the largest magnitude coupling) similarly exhibits relatively small anisotropy (e.g., in the 3Fe form of aconitase, Fe_1 exhibits 10% anisotropy,[87] and in *Av*-Fd I, Fe_1 exhibits ~12% anisotropy[42]).[88] Hence, we may take $A_{iso}(^{57}Fe_1) = A_1(^{57}Fe_1) \pm 10\%$. The Fe_2 site can be completely isotropic, as in aconitase 3Fe,[87] or axial as in *Av*-Fd I, where $\boldsymbol{A}(^{57}Fe) = [9, 21.3, 21.8]$ MHz.[42] In an axial case, the observed spectrum is likely to be dominated by $A_\perp$, which is sufficiently close to A_{iso} simply to assume that $A_{iso}(^{57}Fe_2) \approx A_1(^{57}Fe_2)$. The Fe site with the smallest magnitude spin-projection, Fe_3, in contrast can be very anisotropic (e.g., in the 3Fe form of aconitase, $\boldsymbol{A}(^{57}Fe_3) = [-2.3, -21.9, -7.4]$ MHz to give $A_{iso} = -10.5$ MHz[87] and in *Av*-Fd I, $\boldsymbol{A}(^{57}Fe_3) \approx [-9, 7, 8]$ MHz to give $A_{iso} \approx 2$ MHz[42]) and is thus quite difficult to determine experimentally. Fortunately, for such tensors, $A_{iso}(^{57}Fe_3)$ is very small in magnitude, and thus large percentage errors in this quantity cause no difficulty in using a sum rule introduced below (eq 4) to characterize spin coupling in *Pf*-Fd 3Fe-ox. Thus it is satisfactory to assume that $A_{iso}(^{57}Fe_3) \approx A_1(^{57}Fe_3)$.

The isotropic ^{57}Fe hyperfine constants of a $[Fe_3S_4]^+$ cluster can be used within the theoretical model for spin coupling presented by Kent et al.[57] to deduce the nature of the spin coupling among its three ferric ions ($S(Fe_1) = S(Fe_2) = S(Fe_3) = 5/2$). The spins $S(Fe_2)$ and $S(Fe_3)$ couple (with coupling parameter J_{23}) to give a resultant spin, $S(Fe_{23})$, which is then coupled to $S(Fe_1)$ (with coupling parameters J_{12}, J_{13}) to give the total spin, S_t. There are only two ways to achieve $S_t = 1/2$: $|S(Fe_{23}), S(Fe_1), S_t\rangle = |2, 5/2, 1/2\rangle$ and $|3, 5/2, 1/2\rangle$. If Fe_1 interacts equally with the other two ferric ions ($J_{12} = J_{13}$), then a pure $|2, 5/2, 1/2\rangle$ ground state is obtained. An inequality in the interaction mixes in the $|3, 5/2, 1/2\rangle$ state. This mixing is parametrized by a coefficient α, such that the range $0 \le \alpha^2 \le 0.25$ includes all solutions: $\alpha^2 = 0$ corresponds to the limiting case, $J_{23} > J_{12} = J_{13} > 0$ and $\alpha^2 = 0.25$ corresponds to the other limiting case, $J_{23} = J_{12} > J_{13} > 0$; values outside this range ($0.25 < \alpha^2 \le 1$) correspond to a relabeling of Fe sites. The mixing affects the site spin expectation values, $\langle S_{iz}\rangle$, as follows:[57,60]

$$\langle S_{1z}\rangle = (7/6) - 2\alpha^2$$

$$\langle S_{2z}\rangle = \alpha^2 - (1/3) - (3)^{1/2}\alpha(1 - \alpha^2)^{1/2}$$

$$\langle S_{3z}\rangle = \alpha^2 - (1/3) + (3)^{1/2}\alpha(1 - \alpha^2)^{1/2} \qquad (2)$$

In turn, the ^{57}Fe hyperfine constants for the individual sites change as a function of the spin-coupling scheme

$$A_{iso}(^{57}Fe_i) = K_i\, a_i = 2\langle S_{iz}\rangle a_i \; (i = 1, 2, 3) \qquad (3)$$

where a_i is the isotropic hyperfine coupling for the uncoupled ^{57}Fe site i (site value) and K_i is the spin-projection coefficient for that site ($\sum K_i \propto 1$). Previous workers have found that the site coupling has a value between -18 and -20 MHz (e.g., Kent et al. found $a_i = -20$ MHz[57] and Mouesca et al. report -18.0 and -18.5 MHz as generic site values for Fe^{3+} [60]).

The site value, a_i, and the mixing coefficient, α^2, for *Pf*-Fd 3Fe-ox have been determined by comparing the measured values of $A_{iso}(^{57}Fe^{3+}{}_i)$ to their predicted values calculated with eqs 2 and 3 as a function of α^2. A supportive feature of this process is that the procedure was performed using a wide range of site constants, $-25 < a_i < -6$ MHz, but only $a_i = -19 \pm 1$ MHz gives acceptable fits. The resulting plot is shown in Figure 3, where the shaded horizontal bars are centered at the experimentally observed couplings, and their width represent the experimental uncertainties in these measurements: ± 1 MHz for $A_{iso}(^{57}Fe^{3+}{}_1)$ and ± 2 MHz for $A_{iso}(^{57}Fe^{3+}{}_{2,3})$. While one may make the plot with the full range, $0 \le \alpha^2 \le 1$ (Figure 3, inset), the range of unique solutions is $0 \le \alpha^2 \le 0.25$.[57] Comparison of the experimental value of $A_{iso}(^{57}Fe^{3+}{}_i)$, $i = 1-3$, with the calculated curve of Figure 3 gives $\alpha^2 \approx 0.09(2)$ for *Pf*-Fd 3Fe-ox. This quantitative description of the ground state is in agreement with the qualitative conclusions drawn from ambient temperature, fluid solution NMR measurements.[33]

This description yields the signs for the observed $A_{iso}(^{57}Fe^{3+}{}_{1-3})$: $-37.5(1.0)$, $+26(2)$, and $-11(2)$ MHz. To corroborate this analysis, and more importantly, for subsequent use in assigning valencies in the reduced 4Fe cluster, we introduce the parameter, a_{test}, which was defined by Mouesca et al.[60] and corresponds to the average site isotropic coupling constant for an Fe_n cluster:

$$a_{test} = \sum A_{iso}\mathrm{expt}(^{57}Fe_i) = \sum K_i a_i \; (i = 1, ..., n) \qquad (4)$$

The value, $a_{test} = -22$ MHz, calculated from these results for *Pf*-Fd 3Fe-ox is quite typical for $[Fe_3S_4]^+$ clusters and many other $[Fe_nS_m]$ systems: $a_{test} = -21$ MHz $\pm$ 15%[60] (see Tables I and II).

The derived value for *Pf*-Fd 3Fe-ox, $\alpha^2 \approx 0.09$, is appreciably larger than that observed for other 3Fe Fd's (e.g., $\alpha^2 = 0.01$ for *A. vinelandii* Fd-I[57] as shown by the dotted line in Figure 3). This means that, while *Pf*-Fd 3Fe-ox has the same spin-coupling scheme as other 3Fe Fd's, this protein shows a noticeable difference in the details of the spin coupling among the ferric ions, with $J_{12} \neq J_{13}$, while the other 3Fe Fd's show more nearly equivalent interactions between ions, with $J_{12} \approx J_{13}$. This difference is experimentally manifest in the relatively large value for $\{A_{iso}(^{57}Fe^{3+}{}_2) - A_{iso}(^{57}Fe^{3+}{}_3)\}$ (see Table 1).

^{57}Fe ENDOR of *Pf*-Fd 4Fe-red and *Pf*-Fd 4Fe−CN. CW 35 GHz ENDOR spectra were taken at magnetic field positions across the absorption envelope of the $S = 1/2$ state of the singly and triply labeled *Pf*-Fd-4Fe-red and *Pf*-Fd 4Fe−CN ($[^{57}FeFe_3S_4]^+$ and $[Fe^{57}Fe_3S_4]^+$). All samples exhibit strong ^{57}Fe resonances in the 5−25 MHz region that are absent in natural-abundance samples.

Fe_a: We first focus on the ENDOR patterns for the $[^{57}FeFe_3S_4]^+$, in which only the unique Fe site is enriched. The spectrum from *Pf*-Fd-4Fe-red taken at g_2 (Figure 4A) is dominated by a strong signal at ~18 MHz, which we assign to the ν_+ partner of the single ^{57}Fe site, to yield $A_2(^{57}Fe_a) \approx 34(1)$ MHz using eq 1. No experimental conditions that also allowed definitive observation of the ν_- partner were found; this

(87) Surerus, K. K.; Kennedy, M. C.; Beinert, H.; Münck, E. *Proc. Natl. Acad. Sci. U.S.A.* **1989**, *86*, 9846−9850.

(88) The Fe_1 signal in *Pf*-Fd 3Fe-ox has quite different ENDOR relaxation behavior from the other two ($Fe_{2,3}$), as seen in **Figure S1**, which may be a consequence of spin coupling phenomena.

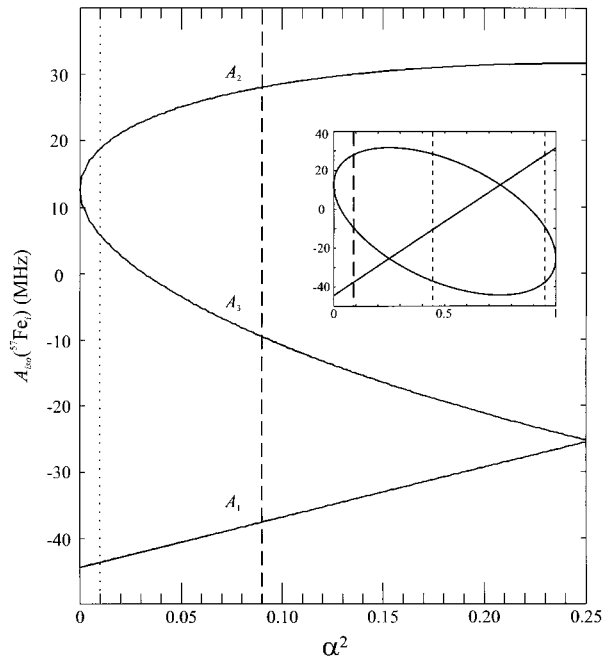

Figure 3. Theoretical $A_{iso}(^{57}Fe_i)$ values for a $[Fe_3S_4]^+$ cluster calculated as a function of the state mixing parameter α^2 according to eqs 2 and 3 using $a(^{57}Fe^{3+}{}_i) = -19.0$ MHz. The main figure shows the range $0 \le \alpha^2 \le 0.25$, which is the physically meaningful range (see text); the inset shows the entire range $0 \le \alpha^2 \le 1$. The shaded bars indicate the experimentally observed couplings for *Pf*-Fd 3Fe-ox (see Table 2). The bar width corresponds to the experimental precision of ±1 MHz for A_1 and ±2 MHz for A_2 and A_3. The vertical dashed line in the main figure indicates the value of α^2 that fits the observed data; those in the inset indicate all three solutions, of which only that at ~0.09 is meaningful (see text). The vertical dotted line in the main figure indicates the value of α^2 (0.01) that fits the data for oxidized *Azotobacter vinelandii* Ferredoxin I.[57]

Table 1. Experimental and Theoretical Isotropic ^{57}Fe Hyperfine Coupling Constants for $[Fe_3S_4]^+$ Clusters

$[Fe_3S_4]^+$ cluster	A_{iso} $(Fe^{3+})_3$[a] (MHz)	a_{test}[b] (MHz)
Pf-Fd 3Fe-ox	−37.5(1.0), +26(2), −11(2)[g]	−22
Dg-H_2ase 3Fe[c]	−44, +20, ~+3 (form 1) −39, +23 (form 2)	−21
Av-Fd I-ox[d]	−41.9, +17.4, +2	−22.5
$[Fe_3S_4]^+$, $S_t = 1/2$, theory case *a*: $\|2, 5/2, 1/2\rangle$[e]	−42, +12, +12	−18
$[Fe_3S_4]^+$, $S_t = 1/2$, theory case *b*: $\|3, 5/2, 1/2\rangle$[f]	+30, −24, −24	−18

[a] Absolute signs are given where available; either from the ENDOR analysis done here or directly from Mössbauer spectroscopy. [b] Average site constant as given by eq 4 as defined by Mouesca *et al.*[60] [c] *Dg*-H_2ase refers to *Desulfovibrio gigas* hydrogenase 3Fe, which exhibits two forms by EPR. ENDOR data are presented.[84] [d] *Av*-Fd I refers to *Azotobacter vinelandii* Ferredoxin I, which has been studied in both the reduced and oxidized state. Mössbauer data from the most recent study are presented.[42] [e] This calculation uses the following parameters in eqs 2 and 3 for $[Fe_3S_4]^+$, $S_t = 1/2$, $\alpha^2 = 0$: $a(Fe^{3+})_3 = -18.0$ MHz, $K(Fe_1{}^{3+}) = +2.33$ (+7/3), $K(Fe_{2,\ 3}{}^{3+}) = -0.67$ (−2/3). The notation $|2, 5/2, 1/2\rangle$ refers to $|S(Fe_{23}{}^{3+}), S(Fe_1{}^{3+}), S_t\rangle$. [f] This calculation uses the following parameters in eqs 2 and 3 for $[Fe_3S_4]^+$, $S_t = 1/2$, $\alpha^2 = 1$: $a(Fe^{3+})_3 = -18.0$ MHz, $K(Fe_1{}^{3+}) = -1.67$ (−5/3), $K(Fe_{2,\ 3}{}^{3+}) = +1.33$ (+4/3). [g] Only the tensor components at g_1 can be determined.

phenomenon has been previously observed in aconitase.[40] The baseline dip at ~10−15 MHz is likely due to natural-abundance ^{57}Fe at the other sites (see below), as often seen in Fe−S proteins,[89] but may include a contribution from the ν_- partner. A similar ^{57}Fe ENDOR signal is observed across the EPR envelope (Figure S2), which yields a hyperfine tensor of

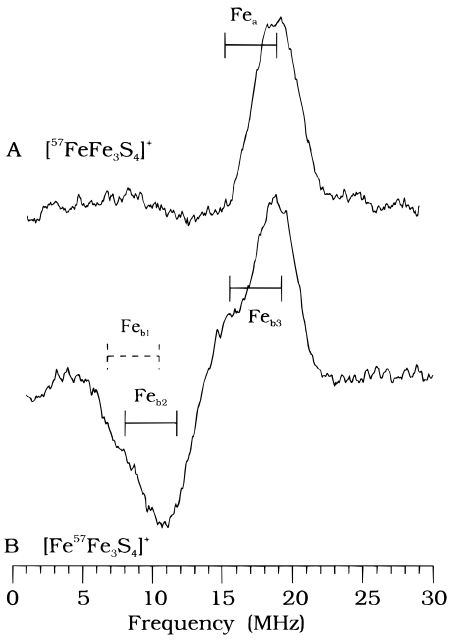

Figure 4. Q-Band CW ^{57}Fe ENDOR of *Pf*-Fd 4Fe-red isotopologs: (A) singly labeled $[^{57}FeFe_3S_4]^+$ and (B) triply labeled $[Fe^{57}Fe_3S_4]^+$ at the maximum EPR signal intensity (g_2). *Experimental conditions*: (A) temperature, 2 K; microwave frequency, 34.887 GHz; microwave power, 20 μW (40 dBm); magnetic field, 1.3340 T ($g = 1.868$, g_2); 100 kHz field modulation amplitude, 0.42 mT; time constant, 32 ms; rf scan rate, −1 MHz/s; rf power, 20 W; number of scans, 40; (B) as in (A) except: microwave frequency, 35.269 GHz; microwave power, 200 μW (30 dBm); magnetic field, 1.3500 T ($g = 1.867$, g_2); 100 kHz field modulation amplitude, 0.33 mT; rf scan rate, −2 MHz/s; number of scans, 500. The "goalposts"correspond to $2\nu(^{57}Fe) = 3.7$ MHz. Solid line goalposts indicate likely assignments of the Fe_a site in (A) and Fe_{b2} and Fe_{b3} sites in (B); the dashed line goalpost gives a tentative assignment for the Fe_{b1} site in (B) based on a_{test} as discussed in the text.

$\boldsymbol{A}(^{57}Fe_a) \approx [28(1), 34(1), 30(2)]$ MHz for the unique, Fe_a, site. This small degree of anisotropy (~10%) is often the case in $[Fe_4S_4]^+$ clusters (see Table SI for a summary of tensors).

Figure 5A shows the Q-band CW ENDOR pattern at g_2 for the singly labeled $[^{57}FeFe_3S_4]^+$-CN isotopolog. A strong signal is observed at ~8.5 MHz corresponding to a ^{57}Fe ENDOR resonance with $A_2(^{57}Fe_a) = 17(1)$ MHz, a value much smaller than that for the same site in *Pf*-Fd-4Fe-red. There is also a weak signal at ~18 MHz that is due to natural ^{57}Fe at other sites (see below); such signals are often seen in Fe−S proteins.[89] ^{57}Fe ENDOR spectra were collected across the EPR envelope and are shown in the Supporting Information (Figure S5). Intensities and line widths are distorted by the relaxation effects discussed in the Experimental Section, but it is possible to describe the main features of the experimental spectra by using the following hyperfine tensor: $\boldsymbol{A}(^{57}Fe_a) = [22(1), 15(1), 14(1)]$ MHz.[90] The simulated spectra are also shown in Figure S5, wherein a relatively narrow ENDOR line width is used so that the individual simulated peak positions can be more readily seen; their maximal intensity matches the corresponding features of the experimental data, which exhibit distorted line shape due to relaxation effects.[91]

(89) Houseman, A. L. P.; Oh, B. H.; Kennedy, M. C.; Fan, C.; Werst, M. M.; Beinert, H.; Markley, J. L.; Hoffman, B. M. *Biochemistry* **1992**, *31*, 2073−2080.

(90) There is a rotation of $\boldsymbol{A}(^{57}Fe)$ about $\boldsymbol{g}$ by the Euler angle $\alpha = 40(10)^o$. This rotation about g_3 was determined using previously described procedures; the nearly axial character of $\boldsymbol{g}$ makes any rotations about g_1 or g_2 difficult to determine.[49−51,73,81]

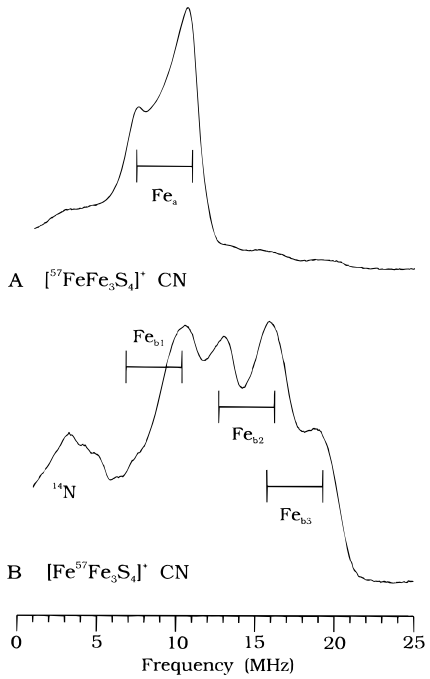

Figure 5. Q-Band CW ^{57}Fe ENDOR of *Pf*-Fd 4Fe−CN isotopologs: (A) singly labeled $[^{57}FeFe_3S_4]^+$ and (B) triply labeled $[Fe^{57}Fe_3S_4]^+$ at the maximum EPR signal intensity (g_2). *Experimental conditions*: (A) temperature, 2 K; microwave frequency, 34.951 GHz; microwave power, 6.3 μW (45 dBm); magnetic field, 1.2800 T ($g = 1.951$, g_2); 100 kHz field modulation amplitude, 0.03 mT; time constant, 32 ms; rf scan rate, −1 MHz/s; rf power, 20 W; number of scans, 20; (B) as in (A) except: microwave frequency, 34.995 GHz; magnetic field, 1.2820 T ($g = 1.950$, g_2); 100 kHz field modulation amplitude, 0.33 mT; average rf power, 5 W, applied in a 10% duty cycle square wave at a 10 kHz repetition rate; number of scans, 40. The "goalposts" indicate $2\nu(^{57}Fe) = 3.52$ MHz and give likely assignments of the Fe$_a$ site in (A) and the three Fe$_b$ sites in (B).

Pulsed (Davies) ENDOR spectra collected at both Q- and X-bands support the CW data analysis. The 35 GHz pulsed data reproduce the peak positions of the Q-band CW study and allows definitive identification of the $\nu_\pm$ partners (data not shown). The X-band data are helpful because the lower microwave frequency causes a corresponding reduction in the ^{57}Fe Larmor frequency ($2\nu(^{57}Fe) = 0.9$ MHz at X-band versus 3.5 MHz at Q-band, for typical conditions employed here). This effectively "collapses" the ENDOR pattern to a single feature at $A(^{57}Fe)/2$.

(Fe$_b$)$_3$: The distribution of structures evidenced in the EPR spectrum of *Pf*-Fd 4Fe-red gives rise to broad and hence poorly resolved ^{57}Fe ENDOR spectra from its triply labeled isotopolog, whereas the well-defined structure of *Pf*-Fd 4Fe−CN, as evidenced by its sharp EPR spectrum (Figure 1C), gives rise to well-resolved ^{57}Fe ENDOR spectra from this isotopolog. For clarity, we therefore begin this subsection with a discussion of the *Pf*-Fd 4Fe−CN $[Fe^{57}Fe_3S_4]^+$ isotopolog.

Figure 5B shows a CW Q-band ENDOR spectrum taken at g_2 for the triply labeled $[Fe^{57}Fe_3S_4]^+$ *Pf*-Fd 4Fe−CN. The signals appearing at <5 MHz are seen in natural-abundance protein and are due to ^{14}N from the cyano ligand[39] and from protein amide nitrogen; the latter type of signal has been described for several Fe−S proteins.[89] These low-frequency signals are not apparent in Figure 5A ($[^{57}FeFe_3S_4]^+$) because they are suppressed by the much lower field modulation amplitude used in that case. The higher-frequency signals in Figure 5B can be assigned to three distinct ^{57}Fe sites, as indicated. Spectra have been collected across the EPR envelope and are shown in Figure S6 and analyzed to obtain the $\boldsymbol{A}(^{57}Fe)$ tensors for the three enriched sites of *Pf*-Fd 4Fe−CN, $[Fe^{57}Fe_3S_4]$ (see Table 2, footnote). In this effort, pulsed (Davies) Q-band ENDOR measurements again were quite helpful in confirming the CW data and assigning $\nu_\pm$ partners.

Figure 4B presents the ^{57}Fe ENDOR spectrum obtained at g_2 from *Pf*-Fd 4Fe-red $[Fe^{57}Fe_3S_4]^+$. Two broad features with opposite phase behavior, as shown in Figures 4B and S4 are observed; one is centered at ∼17 MHz and one at ∼10 MHz. A careful examination of field-dependent spectra (Figure S3) collected under a variety of experimental conditions (Figure S4) allows us to assign the signals of two specific Fe sites, denoted in Figure 4B as Fe$_{b3}$ and Fe$_{b2}$, and to estimate their hyperfine tensors (Table SI). The poor resolution intrinsic to this center, plus the complex dependence of signal shapes on spectrometer settings, precludes an unambiguous assignment of the third site, Fe$_{b1}$. The signals from this one must fall somewhere within the overall ^{57}Fe pattern, which covers a range that corresponds to 12 MHz ≤ $|A_{iso}(^{57}Fe_{b1})|$ ≤ 32 MHz. In the next section the a_{test} sum rule (eq 4) is used to get an approximate value for $A_{iso}(^{57}Fe_{b1})$.

Valency Assignment of Fe Sites of *Pf*-Fd 4Fe-red and *Pf*-Fd 4Fe−CN. Fe$_a$: We begin our assignment of the Fe$_a$ sites in the 4Fe forms of *Pf*-Fd with the two singly enriched isotopologs, as data for these are inherently simpler. We discuss only the isotropic component of the ^{57}Fe hyperfine coupling, as the sum-rule that defines a_{test} is formulated in terms of this quantity. The isotropic hyperfine couplings obtained experimentally for the various Fe sites in the two forms of *Pf*-Fd 4Fe-red are summarized in Table 2 (complete tensors are given in Table SI), which also presents experimental and theoretical $A_{iso}(^{57}Fe)$ values for several $S = 1/2$ $[Fe_4S_4]^+$ clusters. Although we do not directly measure the signs of the $A_{iso}(^{57}Fe)$ in *Pf*-Fd 4Fe-red, the signs can be inferred by comparison of magnitudes to those of other centers for which Mössbauer has provided both signs and magnitudes (Table 2), and these assignments can be tested and confirmed by using the sum-rule provided by the quantity, a_{test}. In such reduced 4Fe Fd ($[Fe_4S_4]^+$) clusters the three ferrous and one ferric ion form one valence-delocalized, or mixed-valence, $(Fe^{2.5+})_2$, pair and one ferrous, $(Fe^{2+})_2$, pair. The data on symmetrically ligated clusters show that the ions of the $(Fe^{2+})_2$ pair have relatively small, positive hyperfine couplings ($A_{iso}(^{57}Fe^{2+}) = +(16-18)$ MHz), while the ions of the mixed-valence pair have larger magnitude, negative hyperfine couplings ($A_{iso}(^{57}Fe^{2.5+}) = -(30-34)$ MHz). We therefore assign the ENDOR signals for the unique, Fe$_a$, site in *Pf*-Fd 4Fe-red and *Pf*-Fd 4Fe−CN as follows: in the native form we take Fe$_a$ to be a member of an $Fe^{2.5+}$ pair, with $A_{iso}(^{57}Fe_a) \approx -31$ MHz, while in the cyanide-bound form we must take Fe$_a$ to be a member of an Fe^{2+} pair with $A_{iso}(^{57}Fe_a) = +17$ MHz.[92]

The conclusion based on the low-temperature ENDOR measurements of the cluster ground state, that Fe$_a$ is one of the $Fe^{2.5+}$ pair in the native state, where it is ligated by Asp carboxylate rather than Cys thiolate, but one of the Fe^{2+} pair

(91) The most accurate determination of the relation between the $\boldsymbol{g}$ and $\boldsymbol{A}(^{57}Fe)$ tensors in a cubane Fe−S cluster has been for a $[Fe_4S_4]^{3+}$ prepared by γ-irradiation of single-crystal $(Et_4N)_2[Fe_4S_4(SCH_2Ph)_4]$.[56] This study showed that the principal axes of the $\boldsymbol{A}(^{57}Fe)$ tensors for the $Fe^{2.5+}$ pair were directed at the inorganic sulfide atoms. The ENDOR data in protein frozen solution precludes determination of the two rotation angles that are likely needed to relate exactly these two tensors. Furthermore, the broad ENDOR line widths and peculiar phase behavior seen here preclude an accurate determination of the orientations of the tensors and precludes the use of TRIPLE resonance techniques, as were successfully employed by Rius and Lamotte to determine relative signs of hyperfine coupling constants.[56]

Table 2. Experimental Isotropic ^{57}Fe Hyperfine Coupling Constants for $[Fe_4S_4]^+$ Clusters

$[Fe_4S_4]^+$ cluster	A_{iso} $(Fe^{2.5+})_2$[a] (MHz)	A_{iso} $(Fe^{2+})_2$[a] (MHz)	a_{test}[b] (MHz)
Pf-Fd 4Fe-red, $S = 1/2$[c]	**−31** (Fe_a), −37 (Fe_{b3})	+21 (Fe_{b2}), ∼+17 (Fe_{b1})	−30
Pf-Fd 4Fe-CN[d]	−25 (Fe_{b2}), −36 (Fe_{b3})	+16 (Fe_{b1}), +**17** (Fe_a)	−28
aconitase (E)[e]	−**39** (Fe_a), −37 (Fe_{b3})	∼+16 (Fe_{b1}), +33 (Fe_{b2}) (av +24.5)	−27
aconitase (ES)[f]	−36 (Fe_{b2}), −40 (Fe_{b3})	∼+16 (Fe_{b1}), +**29** (Fe_a) (av +**22.5**)	−31
*Av*2[g]	−29.7 (×2)	+15.7 (×2)	−28.0
Bs-Fd[h]	−30.7 (×2)	+16.2 (×2)	−29.0
Ec-SiR 4Fe[i]	−33 (×2)	+17 (×2)	−32
$[Fe_4S_4(S\text{-}p\text{-}PhBr)_4]^{3-}$ [j]	−31.8 (×2)	+15.1 (×2)	−33.4

[a] Absolute signs are given where available; either from the ENDOR analysis done here or directly from Mössbauer spectroscopy. Bold face is used to indicate $A(^{57}Fe)$ values of a labile Fe site (Fe_a in *Pf*-Fd and in aconitase). The other Fe sites in *Pf*-Fd and in aconitase are also identified, following Werst *et al.*[40] [b] Average site constant as given by eq 4 as defined by Mouesca *et al.*[60] [c] Tensor values are Fe_a, [−28(1), −34(1), −30(2)] MHz; Fe_{b2}, [22(1), 21(1), 20(1)] MHz; Fe_{b3}, [−43(3), −35(2), −33(1)] MHz. No definitive assignment is possible for Fe_{b1} based on the experimental data; a roughly isotropic tensor with $A_{iso}(^{57}Fe_{b1}) \approx +17(3)$ MHz gives satisfactory values for a_{test} and K_i (see text). [d] Tensor values are Fe_a, [22(1), 15(1), 14(1)] MHz; Fe_{b1}, [12(1), 17(1), 19(1)] MHz; Fe_{b2}, [−20(1), −28(1), −27(1)] MHz; Fe_{b3}, [−32(1), −38(1), −37(1)] MHz. [e] (E) refers to substrate-free reduced aconitase. ENDOR data are presented (with the second choice for $A_{2,3}(^{57}Fe_{b1})$; see Table 1). The assignment of Fe sites to specific oxidation states and choice of signs is based on the analysis of Mouesca *et al.*[60] [f] (ES) refers to reduced aconitase in the presence of substrate. ENDOR data are presented (again with the second choice for $A_{2,3}(^{57}Fe_{b1})$; see Table 1), but sign information from Mössbauer is incorporated.[96] [g] *Av*2 refers to *Azotobacter vinelandii* protein II, $S = 1/2$ state. Mössbauer data in ethylene glycol solvent are used.[46] [h] *Bs*-Fd refers to *Bacillus stearothermophilus* ferredoxin. Mössbauer data are presented.[47] [i] *Ec*-SiR 4Fe refers to *Escherichia coli* sulfite reductase $[Fe_4S_4]^+$ cluster. Mössbauer data are used; ENDOR gives $A_{iso}(Fe^{2.5+}) \approx 37$ and $A_{iso}(Fe^{2+}) \approx 19$ MHz.[97] [j] S-*p*-PhBr refers to *p*-bromothiophenolate. Mössbauer data for $S = 1/2$ state are used.[30]

when it binds cyanide, also has been reached in a high-resolution NMR study of the protein at ambient temperatures.[93] Such a valency conversion was first proposed by Mouesca et al. to occur upon substrate binding in aconitase. The unique iron ion of aconitase, Fe_a, also is four-coordinate in the substrate-free (E) state; it has no protein-derived ligand but has a hydroxo ligand instead of a cysteinyl sulfur. Upon formation of the substrate-bound (ES state of aconitase, Fe_a becomes six-coordinate and this ion exchanges valency with another, Fe_{b2}, so that the net "state swap" is as follows: $(E)Fe_a^{2.5+} \rightarrow (ES)Fe_a^{2+}$, $(E)Fe_{b2}^{2+} \rightarrow (ES)Fe_{b2}^{2.5+}$.[60] While the failure to detect hyperfine-shifted peaks with relaxation properties expected for a ligated Asp14 in the cyanide-bound form is consistent with, but not proof for cyanide replacement of Asp14,[93] based on the comparison to aconitase, we feel it may be useful to leave open the question as to whether cyanide *replaces* the carboxylate of *Pf*-Fd 4Fe, leaving a four-coordinate Fe ion, or whether the cyanide may *add*, in which case the unique Fe site becomes five-coordinate. If the carboxylate of Asp is retained as a ligand, it would imply that the valence distribution within the clusters of both *Pf*-Fd 4Fe and aconitase responds in the same fashion upon increase of coordination number. A higher coordination number for Fe_a, but with the endogenous carboxylato ligand, may be a source of the quite narrow EPR spectrum of *Pf*-Fd 4Fe−CN (indicative of little conformational distribution about the cluster), relative not only to *Pf*-Fd 4Fe-red but also to aconitase (ES). Finally, we observe that in aconitase, which lacks an endogenous ligand, addition of excess cyanide ion leads to cluster decomposition, as monitored by EPR.[94]

$(Fe_b)_3$: Consider first the Fe_b sites in *Pf*-Fd 4Fe−CN. To assign these we rely on comparison with other $S = 1/2$ $[Fe_4S_4]^+$ systems (see Table 2) and on use of the a_{test} parameter (eq 4). These suggest that the two sites with $|A_{iso}(^{57}Fe)| \geq 25$ MHz have negative hyperfine coupling and represent the $Fe^{2.5+}$ pair ($Fe_{b2,\,b3}$). The site with $|A_{iso}(^{57}Fe_{b1})| \approx 16$ MHz, therefore, has a positive sign and together with Fe_a makes up the Fe^{2+} pair. This assignment is confirmed by noting that it yields $a_{test} = -28(2)$ MHz, which is typical for $[Fe_4S_4]^+$ clusters[60] (e.g., $a_{test} = -28.0$ MHz for *A. vinelandii* Fd II,[46] and −31.0 MHz for aconitase (ES)[40]).

We finally deal with the Fe_b sites in *Pf*-Fd 4Fe-red. The Fe_{b3} site has $|A_{iso}(^{57}Fe_{b3})| \geq 30$ MHz, and comparison with other clusters shows that Fe_{b3} makes up the $Fe^{2.5+}$ pair together with Fe_a, with both having negative hyperfine couplings. The Fe_{b2} site, with much smaller magnitude coupling, $|A_{iso}(^{57}Fe_{b2})| \approx 20$ MHz, and opposite phase behavior to that of Fe_{b3}, can therefore be assigned as an Fe^{2+} ion with a positive hyperfine coupling. This means that Fe_{b1} must be also a ferrous site and thus have positive hyperfine coupling. Although the poor resolution of the experimental spectra precludes a direct determination of $A_{iso}(^{57}Fe_{b1})$, the a_{test} sum rule provides an approximate value for this quantity. For typical $[Fe_4S_4]^+$ clusters, a_{test} falls in the range, −(−33−27) MHz (see Table 2).[60] Thus, if we take a_{test}-(*Pf*-Fd 4Fe-red) $\approx -30 \pm 3$ MHz, then eq 4 can be solved using the isotropic hyperfine couplings for Fe_a, Fe_{b2}, and Fe_{b3} to give $A_{iso}(^{57}Fe_{b1}) \approx +17(3)$, which means that the signals from this site fall in the lower frequency region of the observed ^{57}Fe ENDOR pattern (as indicated in Figures 4, S3, and S4).

Spin Coupling Schemes for *Pf*-Fd 4Fe-red in Native and Cyanide-Bound Forms. The $S = 1/2$ ground state of a reduced 4Fe Fd ($[Fe_4S_4]^+$) cluster is achieved by exchange interactions in which the spins of the two ions within a mixed-valence pair order ferromagnetically to form a resultant pair spin, $S((Fe^{2.5+})_2)$, those of the ferrous pair couple to form another resultant spin, $S((Fe^{2+})_2)$, and then the two pair spins couple to yield the total cluster spin,[30,47,60,62,63,66,67] $S_t = 1/2$, of the ground state that is of interest here. As discussed by Mouesca et al.,[60] there are three viable spin coupling schemes that can give rise to this state: $|S((Fe^{2.5+})_2), S((Fe^{2+})_2), S_t\rangle = |9/2, 4, 1/2\rangle$ (case *d*), $|7/2, 3, 1/2\rangle$ (case *e*), and $|5/2, 2, 1/2\rangle$ (case *f*). Each of these is characterized by distinct values for the spin-projection coefficients, K_i, as listed in Table 3. Experimental spin-projection

(92) Preliminary Mössbauer data for *Pf*-Fd 4Fe−CN further supports this assignment; it shows that the unique site of $[^{57}FeFe_3S_4]^+$ in fact has a positive hyperfine coupling whose magnitude is in rough agreement with that reported here.[95]

(93) Calzolai, L.; Gorst, C. M.; Bren, K. L.; Zhou, Z. H.; Adams, M. W. W.; La Mar, G. N. *J. Am. Chem. Soc.* **1997**, *119*, 9341−9350.

(94) Telser, J.; Kennedy, M. C.; Beinert, H.; Hoffman, B. M. Unpublished results.

(95) Ravi, N.; Münck, E. Manuscript in preparation.

(96) Kent, T. A.; Emptage, M. H.; Merkle, H.; Kennedy, M. C.; Beinert, H.; Münck, E. *J. Biol. Chem.* **1985**, *260*, 6871−6881.

(97) Cline, J. F.; Janick, P. A.; Siegel, L. M.; Hoffman, B. M. *Biochemistry* **1986**, *25*, 4647−4654.

Table 3. Experimental and Theoretical Spin-Projection Coefficients ($K(Fe_i)$) for $S = 1/2$ $[Fe_4S_4]^+$ Clusters

$[Fe_4S_4]^+$ cluster	$K(Fe^{2.5+})_2$	$K(Fe^{2+})_2$
Pf-Fd 4Fe-red, $S = 1/2$[a]	+1.51(10)	−1.0(2)
Pf-Fd 4Fe-CN	+1.36(5)	−0.89(10)
aconitase (E)[b]	+1.68	−1.18
aconitase (ES)	+1.69	−1.19
semiempirical[c]	+1.35	−0.85
$[Fe_4S_4]^+$, $S_t = 1/2$, theory case *d*: $\|9/2, 4, 1/2\rangle$[d]	+1.83 (+11/6)	−1.33 (−8/6)
$[Fe_4S_4]^+$, $S_t = 1/2$, theory case *e*: $\|7/2, 3, 1/2\rangle$	+1.50 (+9/6)	−1.00 (−6/6)
$[Fe_4S_4]^+$, $S_t = 1/2$, theory case *f*: $\|5/2, 2, 1/2\rangle$	+1.17 (+7/6)	−0.67 (−4/6)

[a] Uncertainties in K_i values are based on uncertainties in ENDOR data as given in Table 2. For *Pf*-Fd 4Fe-red, $K(Fe^{2+})_2$ incorporates an approximate assigment of $A_{iso}(^{57}Fe_{b1})$ using the a_{test} and $\sum K_i$ constraints (see text). [b] The assignment of Fe sites to specific oxidation states in aconitase is based on the analysis of Mouesca *et al.*[60] who provided the theoretical values. ENDOR data of Werst *et al.* are used.[40] [c] Calculation by Mouesca *et al.*[60] for an idealized $[Fe_4S_4(SR)_4]^{3-}$ cluster. [d] The notation $|9/2, 4, 1/2\rangle$ refers to $|S(Fe^{2.5+})_2, S(Fe^{2+})_2, S_t\rangle$. The decimal values for the spin-projection coefficients are given together with the actual fractional values (Clebsch-Gordan coefficients) in parentheses.

coefficients can be derived from the experimental values for the $A_{iso}(Fe_i)$ and eq 3, provided the a_i site values are known. As discussed previously,[57,60] and mentioned above in the analysis of *Pf*-Fd 3Fe-ox, values for the a_i site constants of ca. −20 MHz are appropriate for the tetrahedral, sulfur-coordinated Fe ions that make up Fe−S clusters. Extensive work by Mouesca et al. has provided significant refinement to this generic value and led to site values appropriate for an $Fe^{2,2.5,3+}$ ion in a given cluster type.[60] For $S = 1/2$ $[Fe_4S_4]^+$ clusters, they propose $a_i(Fe^{2.5+}) = -22.5$ MHz and $a_i(Fe^{2+}) = -18.0$ MHz; for aconitase: $a_i(Fe^{2.5+}) = -22.5$ MHz and $a_i(Fe^{2+}) = -18.5$ MHz; which values we employ here because of the similarity in Fe coordination between aconitase and *Pf*-Fd.

For *Pf*-Fd 4Fe−CN, we obtain $K(Fe^{2.5+}) \approx +1.36(5)$, $K(Fe^{2+}) \approx -0.89(10)$, which values satisfy the normalization condition: $\sum K_i = 0.94(20) \approx 1$. These coefficients for *Pf*-Fd 4Fe−CN are intermediate between those of cases *e* and *f*, which indicates that upon binding of cyanide ion the ground state is a superposition of $|7/2, 3, 1/2\rangle$ and $|5/2, 2, 1/2\rangle$ (Table 3). Such a mixed state is seen for "normal" $[Fe_4S_4(SR)_4]^{3-}$ clusters, as shown by the exact correspondence of K_i values to a semiempirical calculation made by Mouesca et al. (see Table 3).[60] For *Pf*-Fd 4Fe-red, calculation of spin-projection coefficients provides an alternate to the a_{test} sum-rule (eq 4) in confirming the validity of the Fe site descriptions. The unambiguous assignments to Fe_a, Fe_{b3}, and Fe_{b2} provide $K(Fe^{2.5+}) \approx +1.51(10)$ and $K(Fe_{b2}2+) \approx -1.14(10)$, whence the normalization requirement yields $K(Fe_{b1}{}^{2+}) \approx -0.88(20)$. This value is in good agreement with that determined using $A_{iso}(^{57}Fe_{b1})$ derived above from a_{test}: $K(Fe_{b1}{}^{2+}) \approx -0.92(20)$. We can thus estimate that for *Pf*-Fd 4Fe-red, $K(Fe^{2.5+}) \approx +1.51(10)$, and $K(Fe^{2+}) \approx -1.0(2)$.

These spin-projection coefficients for *Pf*-Fd 4Fe-red correspond roughly to those for the theoretical case *e*, $|7/2, 3, 1/2\rangle$ (Table 3). This may be coincidental, since, as pointed out by a helpful reviewer, a "pure" spin state such as $|7/2, 3, 1/2\rangle$ can only be adequately defined for symmetric cluster composed of two symmetric Fe pairs (Fe^{2+} and $Fe^{2.5+}$). In *Pf*-Fd 4Fe-red, the cluster is necessarily asymmetric, by virtue of its three Cys thiolato and one Asp carboxylato ligand, and as manifest by the EPR line width and spin state behavior described above. It is therefore likely that the native $S = 1/2$ cluster has a mixed spin ground state. Nevertheless, it is a state that is clearly distinct from that for *Pf*-Fd 4Fe−CN, as binding of cyanide as a putative replacement to the carboxylato ligand effects cluster spin coupling as seen for 4Fe clusters with four thiolato ligands (intermediate between cases *e* and *f* ($|7/2, 3, 1/2\rangle$ and $|5/2, 2, 1/2\rangle$). Curiously, even though substrate binding to aconitase causes a valency shift within the cluster, both aconitase (E) and (ES) exhibit a spin state intermediate between cases *d* and *e* ($|9/2, 4, 1/2\rangle$ and $|7/2, 3, 1/2\rangle$).[60] The ambient-temperature NMR studies of Calzolai et al. show increased mean values for the iron spin excitation ($\langle S_z\rangle$), and this was provisionally interpreted as reflecting the presence of the $|9/2, 4, 1/2\rangle$ ground state.[93] The ENDOR results here, combined with the data for aconitase, suggest that the $|7/2, 3, 1/2\rangle$ state is also involved, so that the increase in $\langle S_z\rangle$ seen by NMR may arise from weaker antiferromagnetic coupling and/or from the presence of some population of the $S = 3/2$ state of the cluster at ambient temperatures.

Conclusion

The lability of the unique Fe site in *Pf*-Fd has allowed us to prepare several ^{57}Fe isotopolog cluster forms, and these have been investigated by ^{57}Fe ENDOR spectroscopy. A novel analysis procedure permits the use of this ENDOR data alone to estimate the spin-coupling ground states of both the 3Fe-ox and 4Fe-red $S = 1/2$ proteins. The 3Fe-ox, $S = 1/2$ $[^{57}Fe_3S_4]^+$ protein exhibits EPR and ^{57}Fe ENDOR parameters typical for this cluster type, although the EPR signal is extremely broad, indicative of severe protein conformational distribution.[59,83−85] Analysis of the $A(^{57}Fe)$ values allowed assignment of the major electronic ground state of this cluster to $|S(Fe_{2,3}{}^{3+}), S(Fe_1{}^{3+}), S_t\rangle = |2, 5/2, 1/2\rangle$, as in other 3Fe Fd's. However, the ground state of *Pf*-Fd 3Fe-ox has more mixing of the $|3, 5/2, 1/2\rangle$ state than in other 3Fe Fd's, which appears to arise from a less symmetric coupling among the cluster's ferric ions. This, in turn, may be associated with the extremely broad *g* distribution seen in the EPR spectrum of *Pf*-Fd 3Fe-ox.

The ENDOR experiment allows us to examine selectively the $S = 1/2$ state of the native 4Fe-red form, which is presumed to be the relevant one at physiological conditions based on NMR studies, even in the presence of a preponderance of the unphysiological $S = 3/2$ state.[36] However, the studies are hampered by the very low abundance and extremely broad EPR line width of the $S = 1/2$ state, suggesting that distribution in protein conformation persists even in the 4Fe form. This might be a consequence of variable coordination by the carboxylato ligand. Analysis of the ENDOR-derived ^{57}Fe hyperfine couplings for *Pf*-Fd 4Fe-red suggest that the cluster ground state involves $|S(Fe^{2.5+})_2, S(Fe^{2+})_2, S_t\rangle = |7/2, 3, 1/2\rangle$, but may include contributions from the two other possible $S_t = 1/2$ states. The reduced 4Fe cluster of substrate-free aconitase, which also exhibits a unique, labile tetrahedral Fe site with O-donor ligand(s), has a ground spin state intermediate between $|9/2, 4, 1/2\rangle$ and $|7/2, 3, 1/2\rangle$.[60] In combination with the increased value of $\langle S_z\rangle$ seen at ambient temperatures in high-resolution NMR measurements,[93] these data suggest that the spin ground state of *Pf*-Fd 4Fe-red also involves the $|9/2, 4, 1/2\rangle$ and $|7/2, 3, 1/2\rangle$ states. Binding of cyanide ion to the unique Fe of *Pf*-Fd 4Fe-red leads to major electronic changes, giving *g* values, EPR line widths, and spin ground state (superposition of $|7/2, 3, 1/2\rangle$ and $|5/2, 2, 1/2\rangle$) typical of "normal" 4Fe Fd's and model compounds.[39]

Cyanide binding leads to another significant intracluster electronic change: the unique Fe site shifts from formally $Fe_a{}^{2.5+}$ to $Fe_a{}^{2+}$. This valency change also is detected in solution by

NMR analysis.[93] The sequence-specific NMR assignments further show that the Fe ions ligated by Cys-11, -17, and -56 change from formal valence states of (2^+, 2^+, and 2.5^+) to (2.5^+, 2.5^+, and 2^+), respectively, indicating that the complete electronic structure of the cluster is affected by cyanide binding.[93] A valency interchange from $Fe^{2.5+}$ to Fe^{2+} has been proposed to occur upon the binding of substrate to the unique Fe site of the 4Fe-cluster of aconitase, increasing the coordination number of this ion from four to six.[60] Based on occurrence of similar valency interchanges in aconitase and *Pf*-Fd, we suggest it may be useful to leave open the question as to whether cyanide *replaces* the carboxylate of *Pf*-Fd 4Fe, leaving the Fe ion tetrahedral, or whether the cyanide may *add*, in which case the unique Fe site becomes five-coordinate. The possible retention of the endogenous ligand in a single coordination mode may lead to the narrow protein conformational distribution about the cluster and protect the cluster from decomposition by excess cyanide ion.

Acknowledgment. This work was supported by the NSF (MCB 9507061 to B.M.H., MCB 94-05783 to M.W.W.A., a Research Opportunity Award to J.T., and Research Training Group Award DIR-9014281 to the Center for Metalloenzyme Studies) and the NIH (GM45597 to M.W.W.A. and HL13531 to B.M.H.). We thank Prof. E. Münck and Dr. N. Ravi, both of Carnegie-Mellon University, for communicating unpublished results. We thank two reviewers for helping us to clarify our application of the a_{test} sum rule.

Supporting Information Available: The field-dependent ^{57}Fe ENDOR spectra obtained across the EPR envelopes of *Pf*-Fd 4Fe clusters, the ^{57}Fe ENDOR spectra of *Pf*-Fd 3Fe and 4Fe clusters at various experimental conditions, and a table summarizing the $\boldsymbol{g}$ and the ^{57}Fe hyperfine coupling tensors of $S = 1/2$ $[Fe_4S_4]^+$ clusters (13 pages). See any current masthead page for ordering and Internet access instructions.

JA971546X